RM E51G30

C. 2

RESEARCH MEMORANDUM

PERFORMANCE OF A CASCADE IN AN ANNULAR VORTEX-GENERATING TUNNEL OVER RANGE OF REYNOLDS NUMBERS

By Sidney Thurston and Ralph E. Brunk

Lewis Flight Propulsion Laboratory
Cleveland, Ohio

CLASSIFICATION CANCELLED

Authority J. W. Crowley 12/11/53
EO 10501
By [illegible] 1/11/54
R-7813

CLASSIFIED DOCUMENT

NATIONAL ADVISORY COMMITTEE
FOR AERONAUTICS

WASHINGTON
September 28, 1951

UNCLASSIFIED

NATIONAL ADVISORY COMMITTEE FOR AERONAUTICS

RESEARCH MEMORANDUM

PERFORMANCE OF A CASCADE IN AN ANNULAR VORTEX-GENERATING TUNNEL OVER RANGE OF REYNOLDS NUMBERS

By Sidney Thurston and Ralph E. Brunk

SUMMARY

As part of an investigation of the nature and distribution of losses in a compressor, the Reynolds number effect on the performance of a cascade of compressor blades was examined in an annular vortex-generating tunnel over a range of Reynolds number from 50,000 to 250,000 and at angles of attack of 15° and 25°. Tho mean radius section of the cascade showed a total-pressure deficiency, which could be expected from two-dimensional boundary-layer considerations, while the hub and tip sections showed no evidence of a critical Reynolds number within the range investigated.

The turning angle showed no appreciable variation with change in Reynolds number for either of the angles of attack regardless of the spanwise position of the measuring station.

INTRODUCTION

The low pressures attained at high altitudes are known to have a detrimental effect on engine operation and to decrease the efficiency of the axial-flow compressor by a few percent (reference 1). This effect has been attributed chiefly to the fact that at high altitudes the initial compressor stages operate at very low Reynolds numbers. Although some investigations of the effect of Reynolds number on compressor performance have been carried out, they are limited either to the two-dimensional type (reference 2) or to the investigation of the compressor as a whole (reference 1). Recent investigations of secondary flow (references 3 to 5), however, have shown that this type of flow may have considerable influence in blade passages. The viscous origin of the secondary flow makes it important to investigate the effects of Reynolds number in a three-dimensional configuration in a somewhat more detailed manner than has hitherto been done.

In order to determine the effect of Reynolds number in regions where secondary flows are likely to occur, an investigation was conducted at the NACA Lewis laboratory to determined the distribution of losses downstream of a cascade of 65-(12)10 compressor blades (reference 6) over a range of Reynolds numbers. The tests were made at two angles of attack in an annular vortex-generating tunnel. In order to isolate the Reynolds number effects, Mach number limits were maintained between 0.2 and 0.35.

The blade inlet and outlet conditions are presented as plots of air angle distribution, total-pressure deficiency, and axial velocity ratio. In addition; the wake profiles and pressure distributions for three stations along the blade span are shown. The data are supplemented by visual flow studies of the boundary-layer flow path on the blade surface.

Although the blading twist in the annular cascade was such as to simulate the flow in a stationary compressor row, the data reported herein do not give a completely accurate picture of flow in a compressor stator because the hub rotates in an actual compressor while it is stationary in the vortex tunnel. Another difference between the test tunnel and an actual compressor is that the clearances between the blades and the bounding walls in a compressor stator row are located near the hub while in the vortex tunnel they are near the casing. Since these differences may greatly influence the nature of the secondary flow, caution should be taken in any interpretation of the results obtained as applying to an actual compressor. However, because the investigation was carried out in a vortex-generating tunnel, where the flow more nearly corresponds to that in an actual compressor than does a two-dimensional cascade, the results obtained, although only qualitative, may be expected to indicate the general trends of compressor performance.

APPARATUS AND PROCEDURE

Tunnel

The inlet system for the annular tunnel used in this investigation consisted of an atmospheric air inlet, a flat plate orifice, a plenum tank, and throttle valves. After passing through the throttle valves, the air is deflected radially outward (see fig. 1) in the collector to turn 180° and pass radially inward into the nozzle section. After passing through the straightening vanes at the entrance to the nozzle section the air is given a constant prerotation by a set of airfoil-shaped guide vanes designed according to data of reference 7. The angular orientation of these guide vanes is adjusted by a series of

linkages allowing all the blades to be set with one control arm. The air then progresses in a spiral pattern around the 90° bend in the nozzle section past the suction slots, where boundary layer built up in the nozzle is removed at both the inner and outer walls. After passing through the test section the air enters a collector from which it is drawn into the laboratory exhaust system through two throttle valves.

The blade wheel, the rim of which comprises part of the inner annulus wall at the test section, is mounted on bearings and arranged so that it can be positioned circumferentially with respect to the stationary instruments mounted in the casing. The test-section radial passage height is 3.5 inches, with an inner diameter of 20 inches and and outer diameter of 27 inches. The blade clearance, which is the distance between the blade tip and the outer annulus wall, was 0.015 inch.

Test Grid

The test grid consisted of fifty 65-(12)10 compressor blades each having an $1\frac{1}{2}$-inch chord and a 3.5-inch span with solidities varying from 0.885 at the tip to 1.192 at the hub. The blades were designed to subtract a vortex from the entering vortex conditions at a stagger angle of 45° and an angle of attack of 15° at the mean radius. The design was based on the two-dimensional cascade data of reference 6.

Instrumentation

The total weight flow of the air passing into the tunnel was measured by means of a flat plate orifice according to specifications of reference 8. The amount of air removed through the suction slots was measured by means of a submerged flat plate orifice.

The instrumentation to determine the tunnel performance and inlet conditions to the cascade was located one-half chord upstream of the blade row as indicated in figure 1. Two pitot-static tubes and two claw-type yaw tubes were mounted on the outer casing in radially traversing mounts. The instruments were all mounted on the upper half of the casing. In addition, static-pressure orifices were located at this station on both the inner and outer annulus walls and total-temperature measurements were made by means of a thermocouple.

At the outlet measuring station located one-half chord length downstream of the blades (see fig. 1), two claw-type yaw tubes with integral total-pressure tubes and two C type static wedge probes were

mounted on the outer casing in radially traversing mounts. In addition, three total-pressure rakes consisting of fifteen tubes each spaced 1/8 inch apart curved to their respective radii were fixed on the outer casing at locations corresponding to mean radius, 1/2 inch from the hub and 1/2 inch from the tip. The C type static pressure probes and total-pressure rakes were similar in construction to those described in reference 9. The orientation of the pitot-static tubes and the claw-type yaw tubes was established by the null method. The plane of measurement of the orifices of the rakes was one-half chord downstream of the blades. The angle of each tube of the rake was adjusted to meet the air when the angle of attack of the blades was changed.

Static-pressure orifices were installed along the blade surface in four of the test blades at three radial locations corresponding to 1/2 inch from the tip, mean radius, and 1/2 inch from the hub. Fifteen orifices were installed at each blade section as shown in figure 2. The pressure and suction surface measurements were made in the same passage. Chordwise locations of the static-pressure orifices were leading edge, 5, 10, 20, 40, 60, 80, and 90 percent chord for both the suction and the pressure surfaces of the blade.

Test Procedure

Tests were made over a range of Reynolds numbers at angles of attack at the mean radius of 15° and 25° within Mach number limits of from 0.20 to 0.35. Radial static pressure, total-pressure, and air-angle surveys were made at the inlet station. These inlet survey measurements were made at 17 radial positions across the $3\frac{1}{2}$-inch passage.

At the outlet station, both radial and circumferential surveys were made. The circumferential surveys were made by rotating the blades past the measuring instruments through the 7.2° angular displacement between blades and taking readings every $1/2^\circ$. This procedure was repeated at nine radial locations across the annulus.

At the outlet radial positions, 1/2 inch from the hub, mean radius, and 1/2 inch from the tip, more complete total-pressure measurements were made by means of three rakes, one at each position. Simultaneous readings of the wake data were taken by photographing a manometer board. In order to obtain readings at points between the rake tubes spaced 1/8 inch apart, the blades were rotated past the tubes in increments of $1/4^\circ$ and photographs taken of the manometer board at each position.

Because the flow was fairly uniform through the passage, the outlet air angles were determined by averaging arithmetically the angles determined by the circumferential surveys. The angle variation across the blade wakes was not considered in this average.

In order to discern circumferential variations, duplicate sets of instruments were provided at each axial station. However, preliminary measurements made at different circumferential positions showed that such variations were small. Some measurements were made to compare the rake data with the point-to-point survey measurements. These measurements were also found to be in close agreement except at very low Reynolds numbers. At these low Reynolds numbers, small variations in test conditions which occurred while the measurements were being made caused an appreciable change in the pressures. Therefore, the rake readings are accepted as more nearly representative of the true values, since the time element involved is very small as compared with the time involved in making point-to-point measurements.

Visual Flow Tests

Visual flow tests were made to determine the direction of boundary-layer flow along the blade surface. The technique used was based on the chemical reaction of hydrogen sulfide gas with white lead to produce a dark brown stain. Hydrogen sulfide was selected over other reagents because it has substantially the same molecular weight as air (34) and thus mixes with air rather slowly. The test blades were coated with a thin layer of white lead and the gas was injected through the static pressure orifice at the 10-percent-chord point of the blade at each radial station. Traces were obtained for both the pressure and suction surfaces at each of the three radial locations for blade Reynolds numbers of 50,000 and 125,000 at an angle of attack of 25° at the mean radius.

Turbulence Measurements

Measurements of the intensity of turbulence were made in the tunnel upstream of the blade rows by use of a hot-wire anemometer system designed at the Lewis laboratory. The measurements indicated that the intensity, which varied with the noise level in the tunnel and surrounding areas, was never lower than 1 percent.

Accuracy of Measurement

The pitot-static tube used for upstream surveys, the C type static tube used for downstream surveys, and the claw-type yaw tubes were

calibrated in a steady flow tunnel. On the basis of this calibration, the accuracy of measurement for these tests is estimated as follows (all symbols are defined in appendix A):

P_s	± 0.1 inch water
P_T	± 0.1 inch water
Angle	$\pm 1.0^\circ$

PERFORMANCE AND RESULTS

General Performance

The performance of the annular vortex-generating tunnel is shown in figures 3 and 4. These data were taken at the cascade inlet measuring station located one-half chord length upstream of the stator blade row, over the range of Reynolds numbers from approximately 40,000 to 290,000 for an inlet air angle at mean radius of 45°.

The radial distribution of air angle across the passage is shown in figure 3. The dashed curve shows the air angle distribution that would be required for design conditions of free vortex based on an air angle of 45° at the mean radius. The experimental results show a deviation of 0.7° to 2.5° below design at the hub measuring station, 1/2 inch from the hub, and 0.6° to 1.2° above design at the tip measuring station, located 1/2 inch from the casing. As the angle of attack of the test blades was set on the basis of the inlet air angle distribution which is shown by the dashed line, the angle of attack of the test blades was 0.7° to 1.2° higher at the tip measuring station and 0.6° to 2.5° lower at the hub measuring station. This result would be expected to give a turning angle which is greater than design at the tip station and less than design at the hub station. However, since these angles of attack were reasonably close to the design angles the blades could not be expected to stall because of these small differences. Figure 3 also shows that the variation of Reynolds number has no appreciable effect on the distribution of inlet air angle. In figure 4(a) the ratio of moment of momentum to its maximum value measured across the passage is plotted against the radial passage distance. The ratio of axial velocity to its maximum value measured across the passage is plotted against the radial passage distance as shown in figure 4(b). A total-pressure loss parameter $\Delta P_{T,1}$ is shown in figure 4(c). These plots can be used as a measure of the deviations from free vortex conditions. For a free vortex, $rV_{W,1}/rV_{W,1_{max}}$ and $V_{a,1}/V_{a,1_{max}}$ should be unity and $\Delta P_{T,1}$ should be zero.

The performance of the tunnel, although deviating from true free vortex conditions, is typical of what may be expected in a three-dimensional configuration. The largest deviations occur near the bounding walls. Outside these regions the flow approaches very nearly the true free vortex condition. As in figure 3, the parameters plotted in figure 4 remained nearly the same for all Reynolds numbers investigated.

Cascade Performance

In figures 5 and 6, the performance of the cascade is shown at the outlet measuring station, one-half-chord downstream, with angles of attack at the mean radius of 15° and 25°, respectively. The measured turning angle and the design turning angle adjusted so as to coincide with the measured turning at the mean radius are shown in figure 5. The deviations from the angle distribution required for design conditions indicate that there is a definite underturning of the air at the hub measuring station and that two-dimensional cascade data cannot be directly applied to a three-dimensional configuration without consideration of the regions adjacent to the bounding walls. The slightly greater-than-design angle of attack at the tip position should tend to cause a slight overturning while the less-than-design angle of attack at the hub station should cause a slight underturning. Although the underturning at the hub is actually indicated in figure 5, the magnitude of this underturning is much greater than can be explained by the slightly decreased angle of attack. This phenomenon of underturning in the vicinity of confining walls has been accounted for in the literature as secondary flow (see, for instance, reference 3).

The performance parameters $V_{a,2}/V_{a,2_{max}}$ and $\Delta P_{T,2}$ at the outlet station are shown in figure 6. The measurements plotted in this figure were made along a radial line at half the circumferential spacing between the blades. This figure indicates that a total-pressure and axial velocity deficiency (when compared with the maximum values at this measuring station) occurs near the hub and casing. This deficiency is particularly large near the hub for both 15° and 25° angles of attack at the mean radius. Figure 6 also indicates that at this position in the center of the blade passage (on the nearly radial line midway between two blades) the effect of Reynolds number on the axial velocity ratio and $\Delta P_{T,2}$ is not appreciable.

Effect of Reynolds Number on Turning

In figure 7 the turning angles at the three measuring stations across the blade are plotted against Reynolds number for design angles

of attack of 15° and 25° at the mean radius. With decreasing Reynolds number, no apparent change in turning is indicated beyond the scatter of the data at the hub measuring station. At the mean radius and tip measuring stations a very slight decrease of turning angle with a decrease in Reynolds number may take place; however, because of the large scatter of the data, this variation cannot be considered conclusive.

Pressure Distributions

Some typical pressure distributions obtained are shown in figures 8(a) to 8(f). Figures 8(a) to 8(c) show the pressure distribution for the hub, mean radius, and tip stations respectively for an angle of attack of 15° at Reynolds numbers of approximately 50,000 and 150,000. Figures 8(d) to 8(f) show the pressure distributions for an angle of attack of 25° presented in the same order. The variations in the form of the pressure distribution diagrams with Reynolds number is similar in trend to the variations shown in reference 10. Separation of the flow from the surface of the blade would be expected to be indicated on the pressure distribution diagrams by regions of approximately constant pressure as stated in this reference. In the results of this investigation, these regions of constant pressure may be obscured because of insufficient pressure orifices on the blade surface; some regions of constant pressure can, however, be noted for the diagrams obtained at the low Reynolds numbers.

Wake Profiles

Wake profiles obtained one-half-chord length downstream of the cascade are shown in figure 9. Figures 9(a) to 9(c) show the profiles for the hub, mean radius, and tip position for an angle of attack of 15° at Reynolds numbers of approximately 55,000 and 150,000. Profiles for an angle of attack of 25° are shown in figures 9(d) to 9(f) presented in the same order at Reynolds numbers of approximately 52,000 and 193,000. Figure 9 shows that both at the hub and at the mean radius, the wakes behind the blades were well defined, while near the tip, the shape of the wake profiles is irregular and some total-pressure loss is indicated over the whole blade spacing. This irregularity may have been due to the presence of tip clearance through which flow from the pressure surface onto the suction surface of the blades must have taken place. Attention is called to the fact that the parameter $\Delta P_{T,2}$ is not necessarily indicative of total-pressure loss across the cascade (from inlet to outlet), inasmuch as the total pressure at the inlet was not necessarily equal to the maximum total pressure at the outlet. The parameter $\Delta P_{T,2}$ is used only to show the changes in the wake

characteristics in terms of the conditions prevailing at any given measuring position. Similarly, the area under the curves of figure 9 is indicative of total-pressure deficiency of one spacing at any given measuring position, but not across the cascade. The area under the curve of figure 9 for the low Reynolds number is larger than the area for the high Reynolds number at the tip and mean radius. At the hub measuring station, however, the two areas are approximately the same. This condition is true for both angles of attack.

In order to present the variation of this area with Reynolds number, a total-pressure deficiency coefficient is used. This coefficient is defined as

$$C_{PD} = \frac{1}{S}\int_{0}^{S} \Delta P_{T,2}\, dS$$

and it represents a total-pressure loss for one spacing. The variation of the total-pressure deficiency coefficient with Reynolds number is shown in figure 10 for the hub, mean radius, and tip measuring stations at angles of attack of 15° and 25°.

The variation of total-pressure deficiency coefficient with Reynolds number for an angle of attack of 15° is considered first (fig. 10(a)). At the mean radius, a sudden increase in total-pressure deficiency coefficient is obtained at a Reynolds number of approximately 120,000 as the Reynolds number is decreased. This behavior is as expected from two-dimensional boundary-layer considerations. With a decrease in Reynolds number, more and more of the boundary layer on the blade surface becomes laminar and this laminar boundary layer is unable to sustain the pressure gradient imposed on it. The Reynolds number, at which the sudden increase in total-pressure deficiency coefficient is obtained at the mean radius, can be defined as the critical Reynolds number of the blade section.

No such marked distinction in the behavior of the total-pressure deficiency coefficient with variation of Reynolds number is obtained at either the hub or the tip measuring stations. At the hub measuring station, the total-pressure deficiency coefficient remains essentially constant (the slight maximum indicated is questionable because of the scatter of the data) in the Reynolds number range investigated.

At the tip measuring station the curve of total-pressure deficiency coefficient against Reynolds number shows a slight increase with Reynolds number up to approximately 80,000, and beyond this point the value of the deficiency coefficient drops with further increase of Reynolds number. The highest values of total-pressure deficiency coefficient are obtained at the hub measuring station and the lowest at the mean radius.

The effects of changing the angle of attack from 15° to 25° is shown in figure 10(b). The curves obtained exhibit trends similar to those obtained at an angle of attack of 15°. A critical value of Reynolds number of approximately 145,000 is obtained at the mean radius station. Above this value the total-pressure deficiency coefficient is constant while below this value it increases.

The value of the coefficient at the hub station is again approximately constant. At the tip measuring station, however, for an angle of attack of 25° no maximum value of the total-pressure deficiency coefficient was noted (in the range investigated). The total-pressure coefficient at this measuring station increases continually with a decrease of Reynolds number. The slight tendency of the total-pressure deficiency coefficient to level off at a constant value at high Reynolds numbers cannot be considered conclusive because of the large scatter of the data.

A comparison of the relative magnitudes of total-pressure deficiency coefficient for angles of attack of 15° and 25° (fig. 10) shows that the values of the coefficient at the angle of attack of 25° are consistently higher for each of the measuring stations.

Visual Flow Studies

An additional illustration of the flow processes is obtained by the visual flow studies. A typical set of results is shown in figure 11 for Reynolds numbers of approximately 125,000 and 50,000 at an angle of attack of 25°. The directional characteristics of the traces is upward on the blade suction surface at the hub and mean radius stations and downward at the tip station. These traces essentially show the direction of the boundary-layer flow path along the blade surface. Application of these results to the discussion of total-pressure deficiency coefficient indicates that there may be an effect caused by the upward deflected low-momentum air in the boundary layer at the central portion of the blade and the downward deflected low-momentum air at the tip region which would manifest itself at the point of measurement one-half chord downstream. As the mean radius boundary-layer deflection is seen to progress upward with a decrease in Reynolds number while the tip station deflection remains the same, this effect, which would manifest itself by increased total-pressure deficiences at the tip measuring station, is anticipated to increase with decreasing Reynolds numbers. This upward deflection of low momentum air may be the reason why total-pressure deficiency coefficient at the tip station continues to increase with decreasing Reynolds number for angles of attack of both 15° and 25°.

SUMMARY OF RESULTS

The following results were obtained from an investigation to determine the effects of Reynolds number on a cascade of 65-(12)10 blades in an annular vortex-generating tunnel, at angles of attack of 15° and 25° and Reynolds number variation from approximately 50,000 to 250,000:

1. No appreciable variation in turning angle with change in Reynolds number was noted at the hub, tip, or mean sections of the blade.

2. No critical Reynolds number was apparent within the range investigated at the hub and tip of the blade. At the mean radius, the behavior of the total-pressure deficiency coefficient is similar to what could be expected from two-dimensional boundary-layer considerations.

Lewis Flight Propulsion Laboratory
National Advisory Committee for Aeronautics
Cleveland, Ohio

APPENDIX - SYMBOLS

The following symbols are used in this report:

C_{PD} total-pressure deficiency coefficient, $\frac{1}{S}\int_0^S \Delta P_{T,2}\, dS$

c chord

M Mach number

q average dynamic head, $\frac{1}{2}\frac{(\rho_1+\rho_2)}{2}\left[\left(\frac{V_{a,1}+V_{a,2}}{2}\right)^2+\left(\frac{V_{W,1}+V_{W,2}}{2}\right)^2\right]$

P pressure

P_M mean static pressure, $\frac{P_{s,1}+P_{s,2}}{2}$

ΔP_T local pressure loss coefficient, $\frac{P_{T,max}-P_T}{P_{T,max}-P_s}$

Re Reynolds number $\left(\frac{\rho c V_1}{\mu}\right)_m$

r radius

S circumferential distance between two blades, $\frac{2\pi r}{50}$

V velocity

α angle of attack, angle between entering air and chord line of blade

β air angle, angle between air direction and axial direction of tunnel

θ turning angle, $\beta_1 - \beta_2$

μ absolute viscosity

ρ density

Subscripts:

a axial

L local

m mean radius

max maximum for line survey considered

s	static
T	total
W	tangential
1	inlet station
2	outlet station

REFERENCES

1. Wallner, Lewis E., and Fleming, William A.: Reynolds Number Effect on Axial-Flow Compressor Performance. NACA RM E9G11, 1949.

2. Erwin, John R., and Emery, James C.: Effect of Tunnel Configuration and Testing Technique on Cascade Performance. NACA TN 2028, 1950.

3. Lieblein, Seymour, and Ackley, Richard H.: Secondary Flows in Annular Cascades and Effects on Flow in Inlet Guide Vanes. NACA RM E51G27, 1951.

4. Squire, H. B., and Winter, K. G.: The Secondary Flow in a Cascade of Airfoils in a Nonuniform Stream. Jour. Aero. Sci., vol. 18, no. 4, April 1951, pp. 271-277.

5. Hawthorne, William R.: Secondary Circulation in Fluid Flow. Gas Turbine Lab., M. I. T., May 1950.

6. Bogdonoff, Seymour M., and Bogdonoff, Harriet E.: Blade Design Data for Axial-Flow Fans and Compressors. NACA ACR L5F07a, 1945.

7. Zimney, Charles M., and Lappi, Viola M.: Data for Design of Entrance Vanes from Two-Dimensional Tests of Airfoils in Cascade. NACA ACR L5G18, 1945.

8. Anon.: Fluid Meters, Their Theory and Application. A.S.M.E. Res. Pub., pub. by Am. Soc. Mech. Eng. (New York), 4th ed., 1937.

9. Mankuta, Harry, and Guentert, Donald C.: Investigation of Performance of Single-Stage Axial-Flow Compressor Using NACA 5509-34 Blade Section. NACA RM E8F30, 1948.

10. Pinkerton, Robert M.: The Variation with Reynolds Number of Pressure Distribution over an Airfoil Section. NACA Rep. 613, 1938.

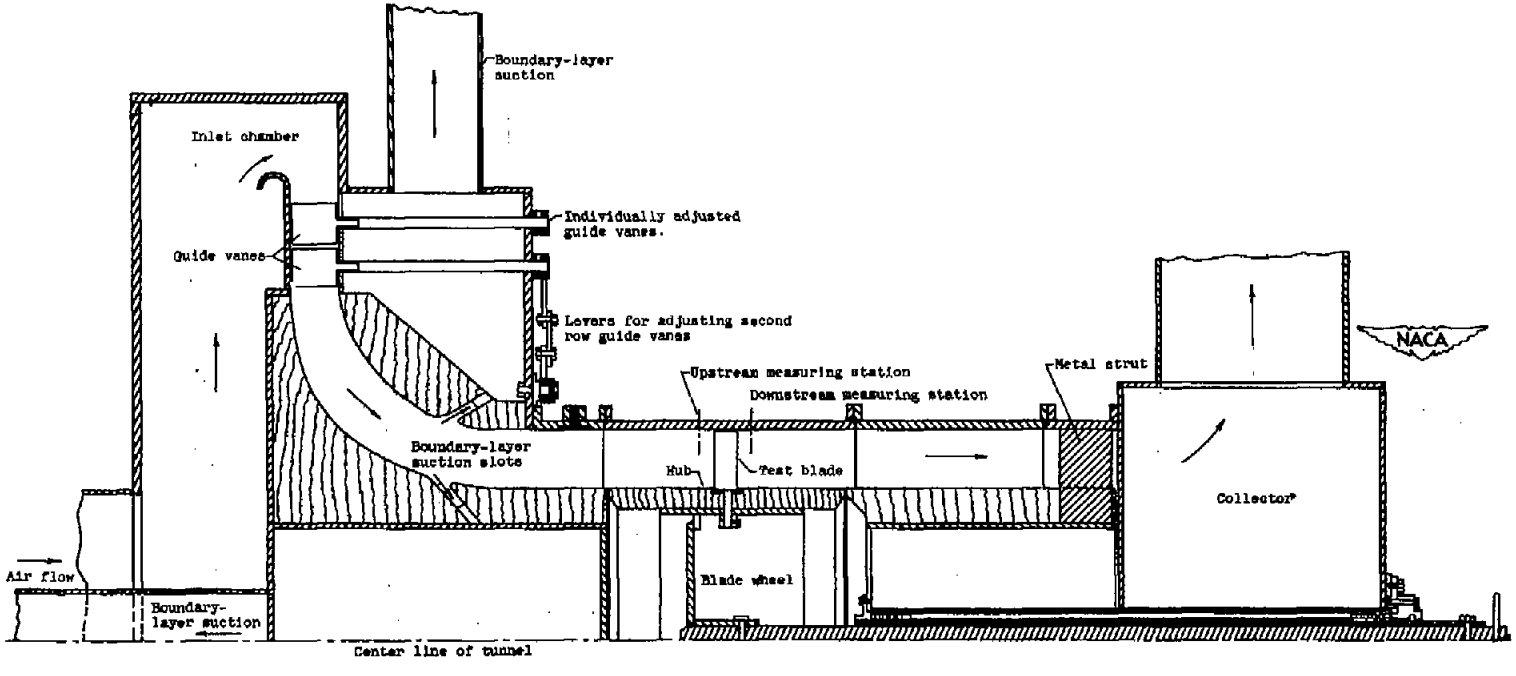

Figure 1. - Sketch of axial-flow compressor blade test rig. (Approximate scale, $\frac{3}{16}$:1.)

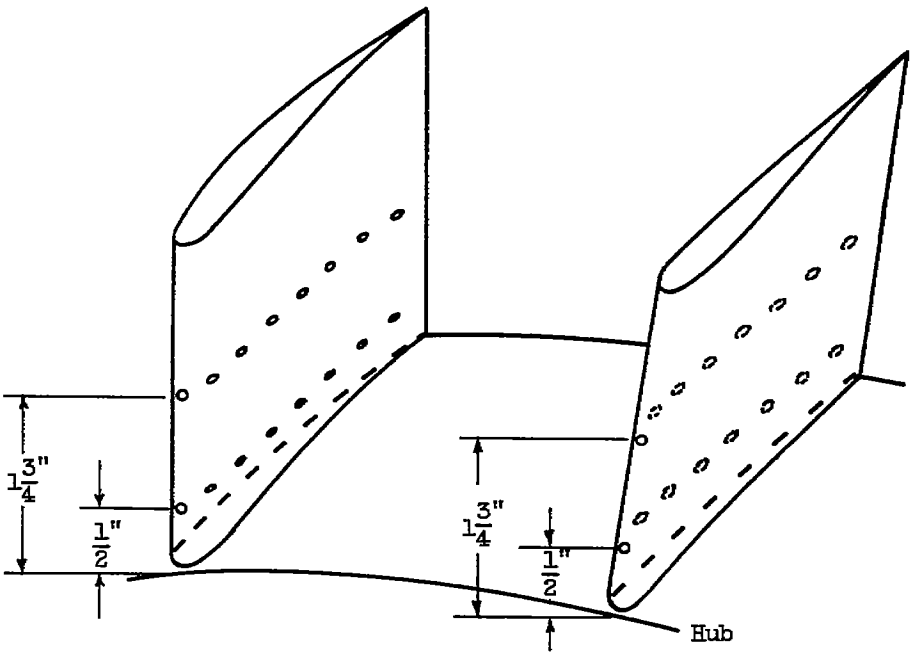

Passage A

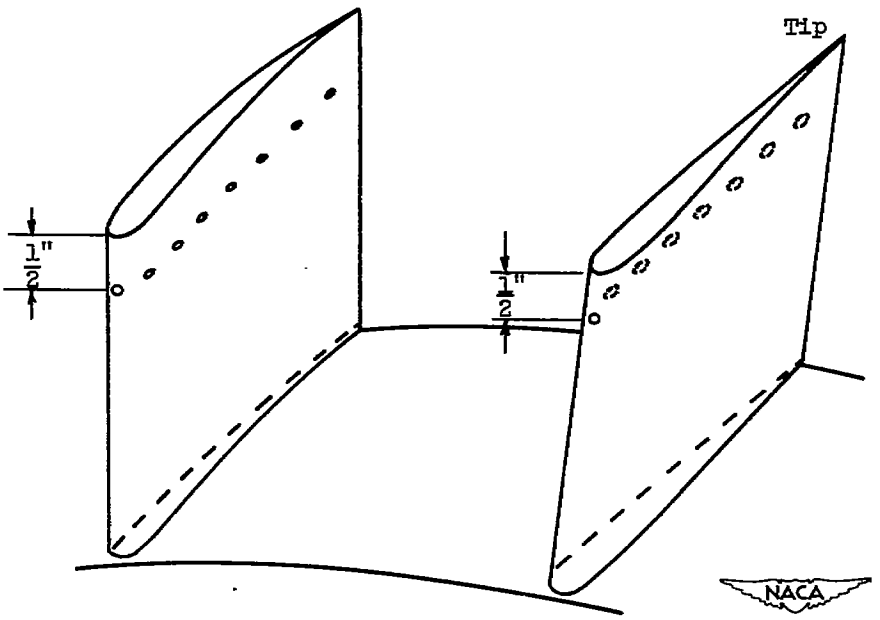

Passage B

Figure 2. - Location of static-pressure holes. (Pressure holes are located at 0, 5, 10, 20, 40, 60, 80, and 90 percent chord.)

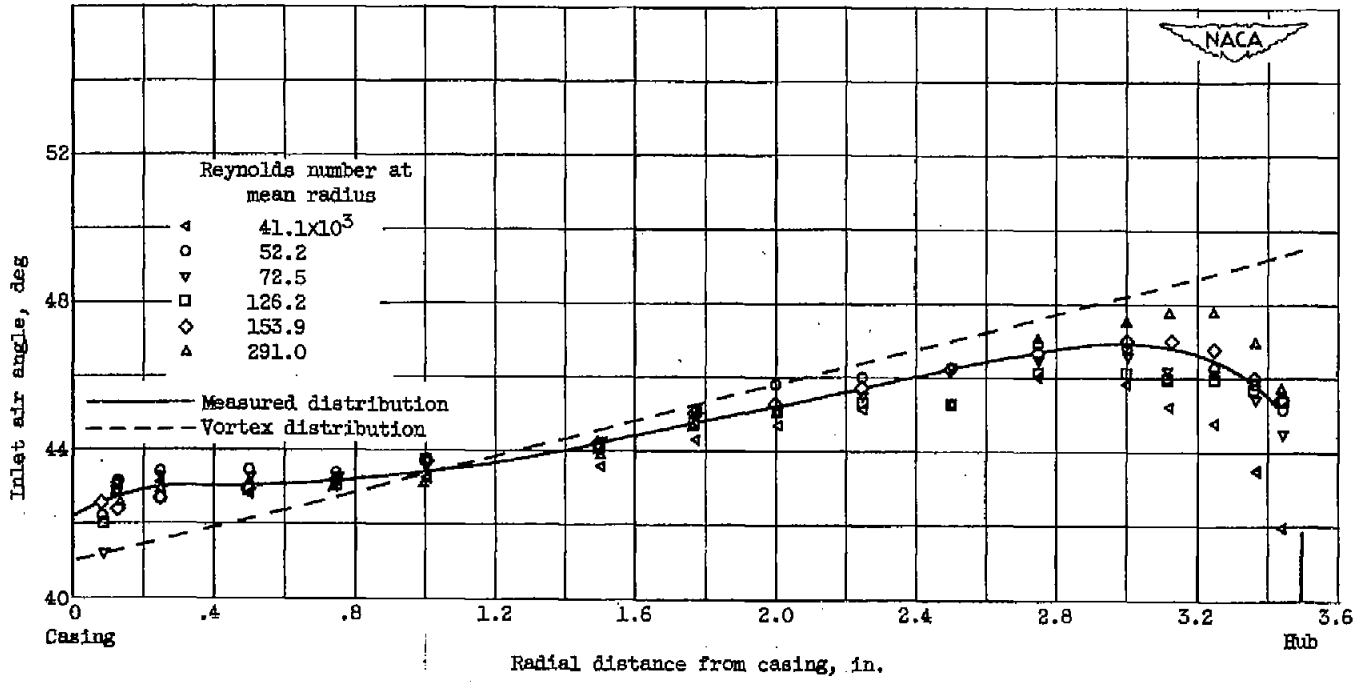

Figure 3. - Radial distribution of inlet air angle.

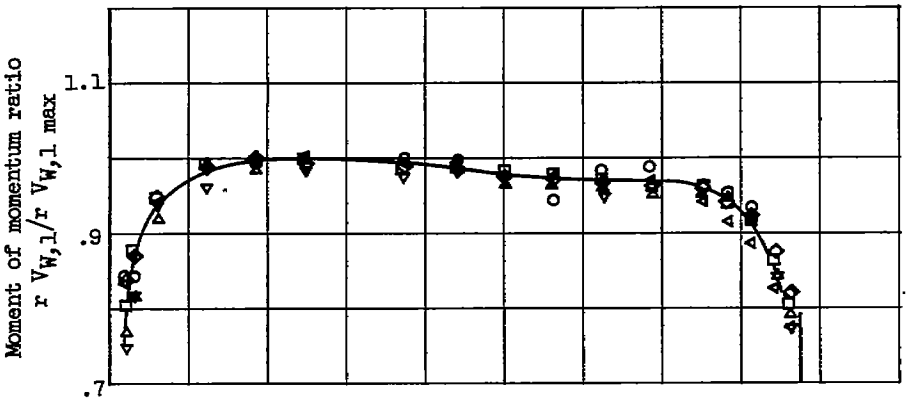

(a) Moment of momentum ratio.

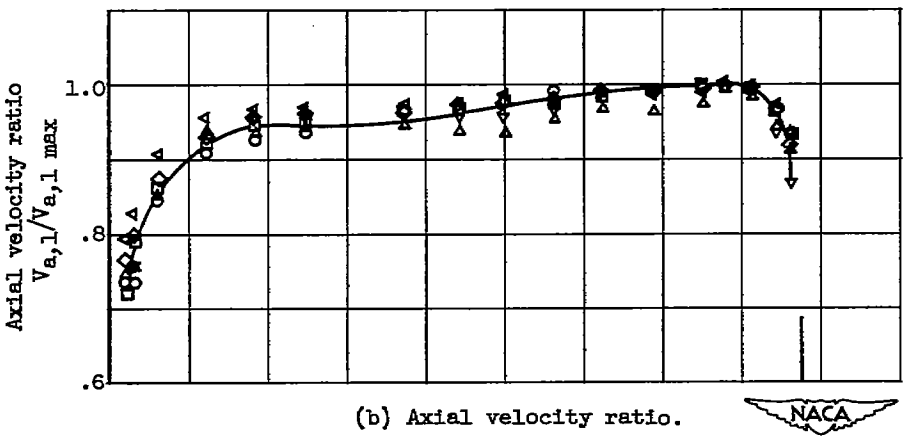

(b) Axial velocity ratio.

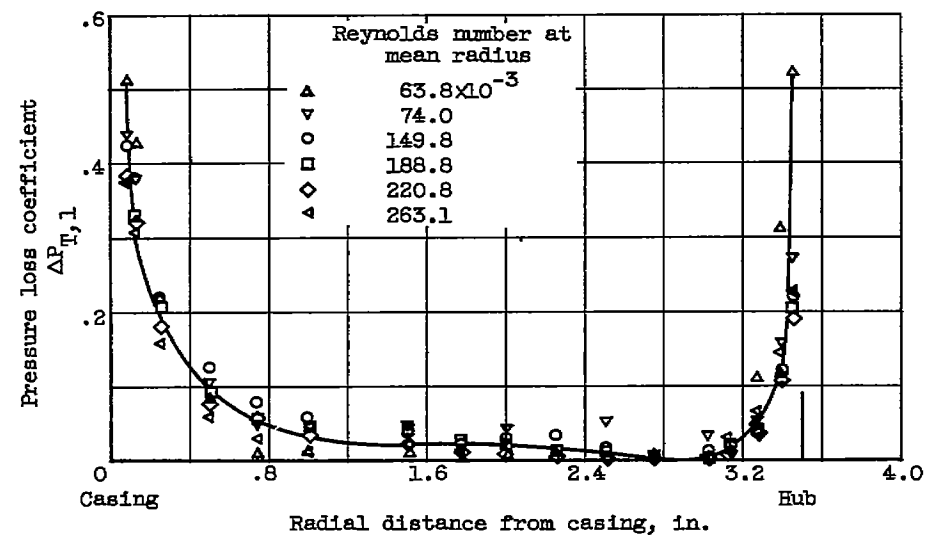

(c) Pressure loss coefficient.

Figure 4. - Radial distribution at inlet.

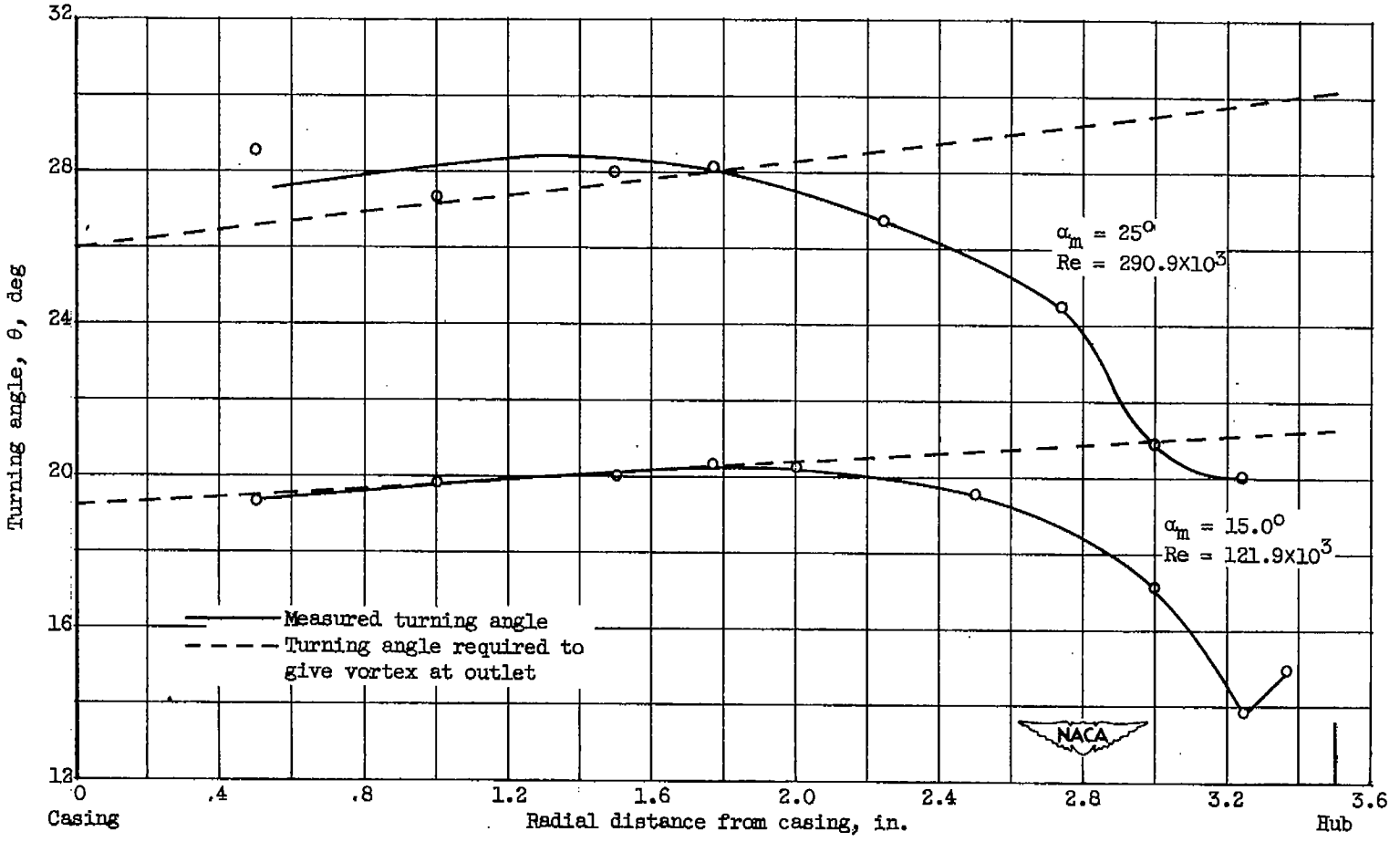

Figure 5. - Radial distribution of turning angle.

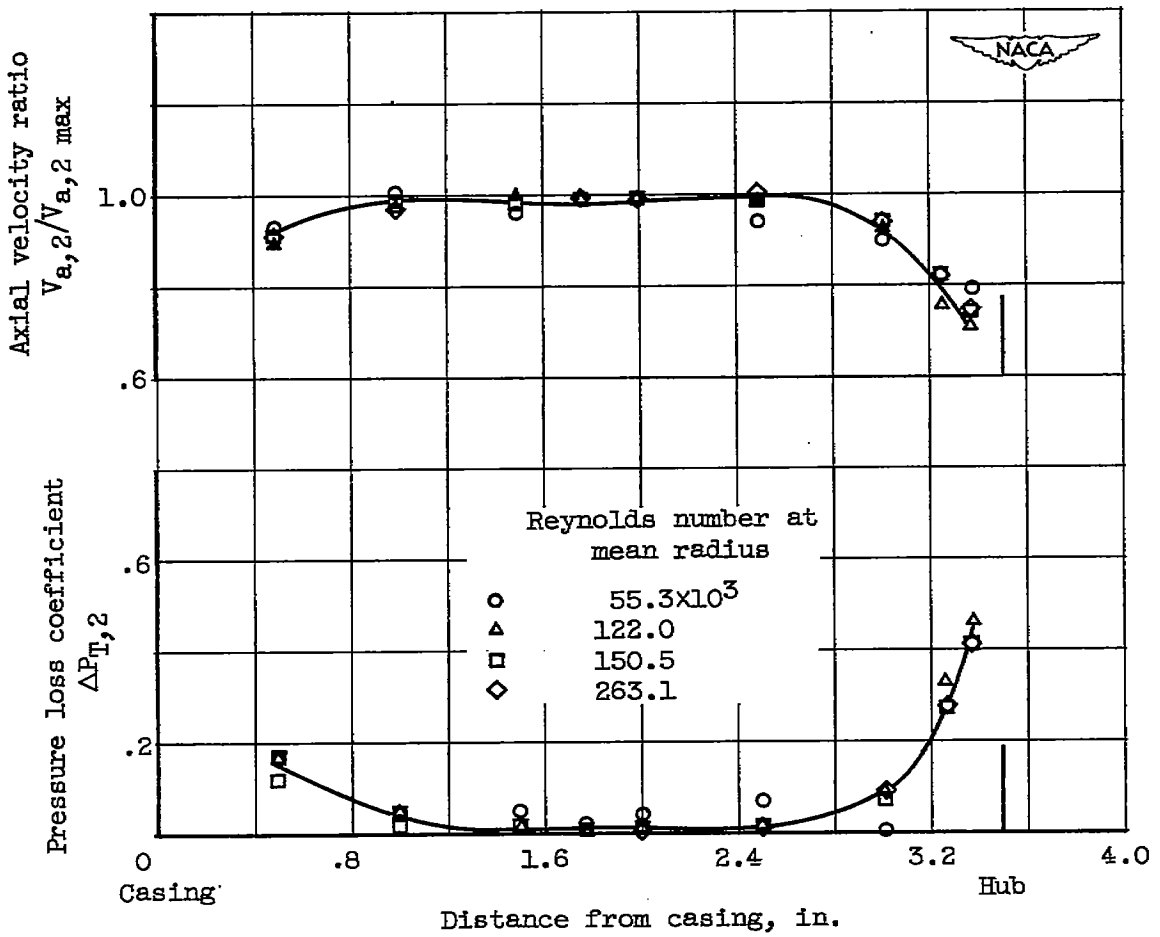

(a) Angle of attack at mean radius, 15°.

Figure 6. - Radial distribution at outlet of axial velocity ratio and pressure-loss coefficient.

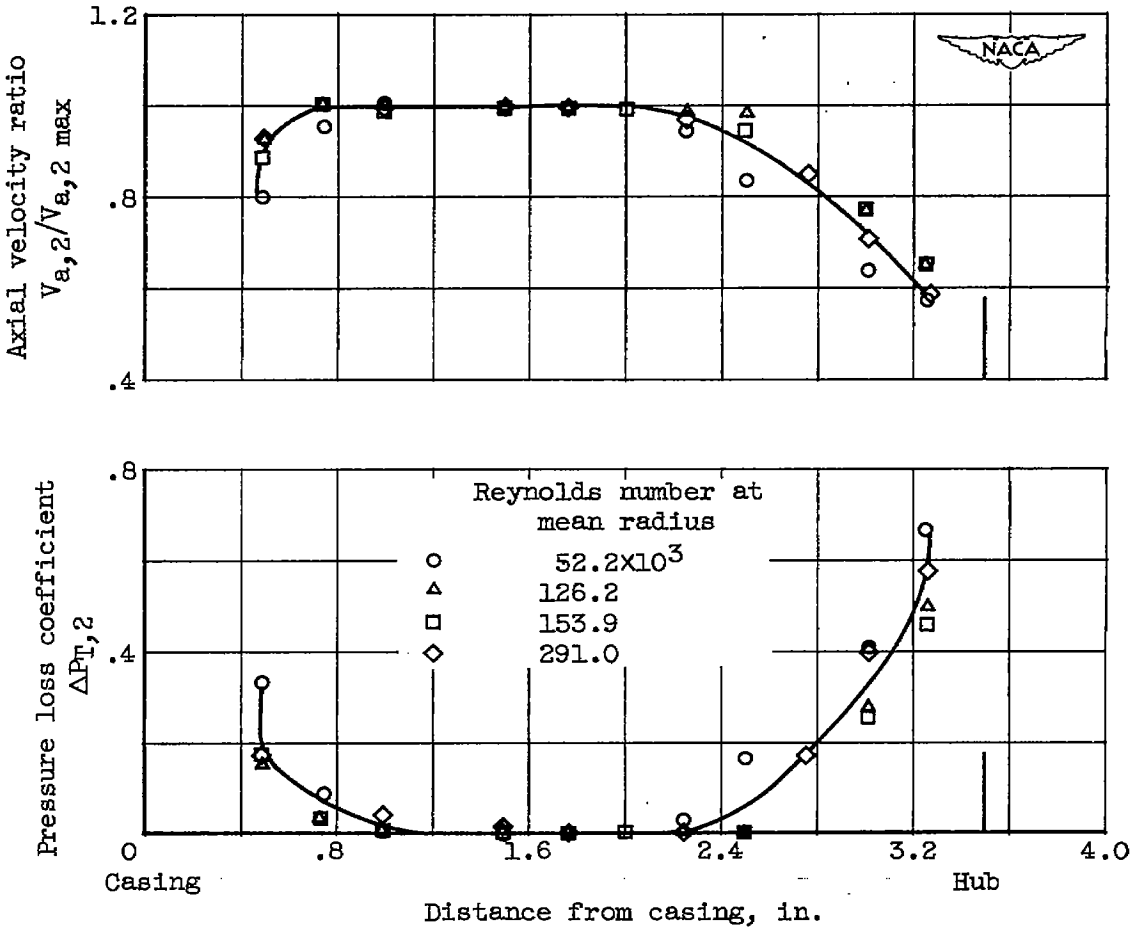

(b) Angle of attack at mean radius, 25°.

Figure 6. - Concluded. Radial distribution at outlet of axial velocity ratio and pressure loss coefficient.

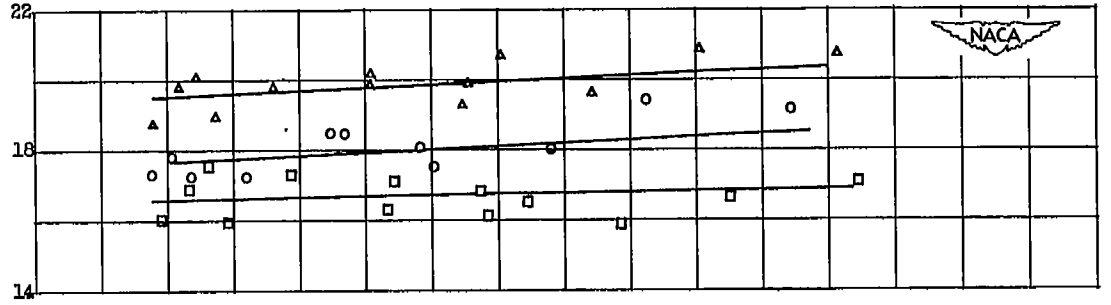

(a) Angle of attack at mean radius, 15°.

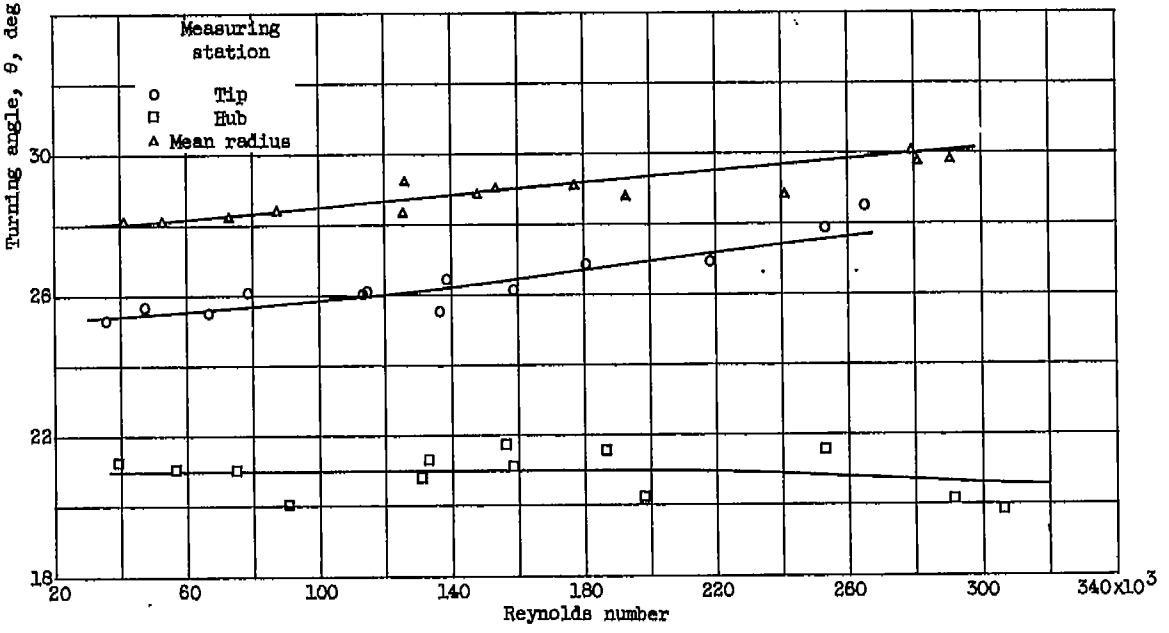

(b) Angle of attack at mean radius, 25°.

Figure 7. - Effect of Reynolds number on turning angle.

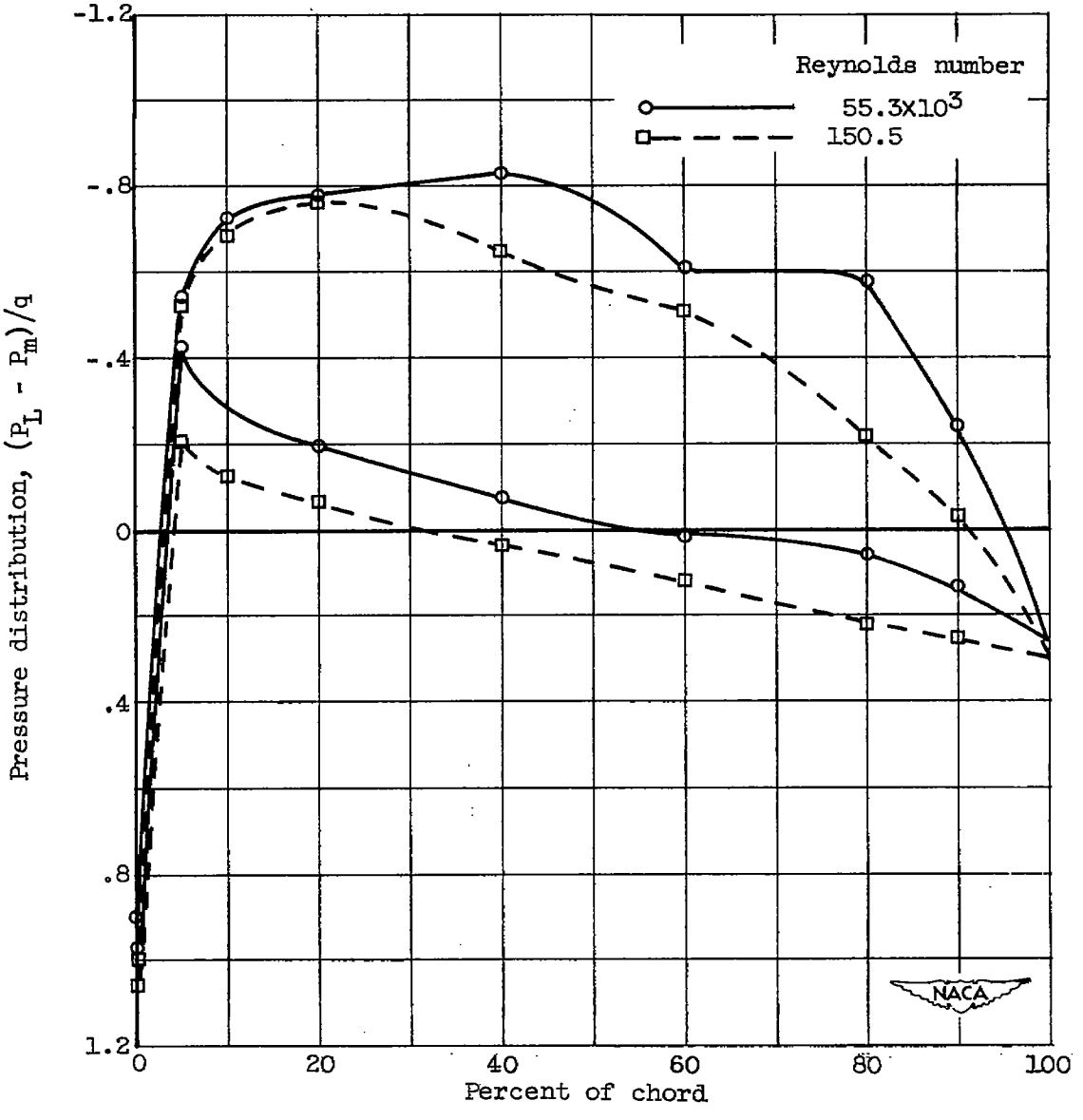

(a) Hub; angle of attack at mean radius, 15°.

Figure 8. - Pressure distribution around 65-(12)10 compressor blades.

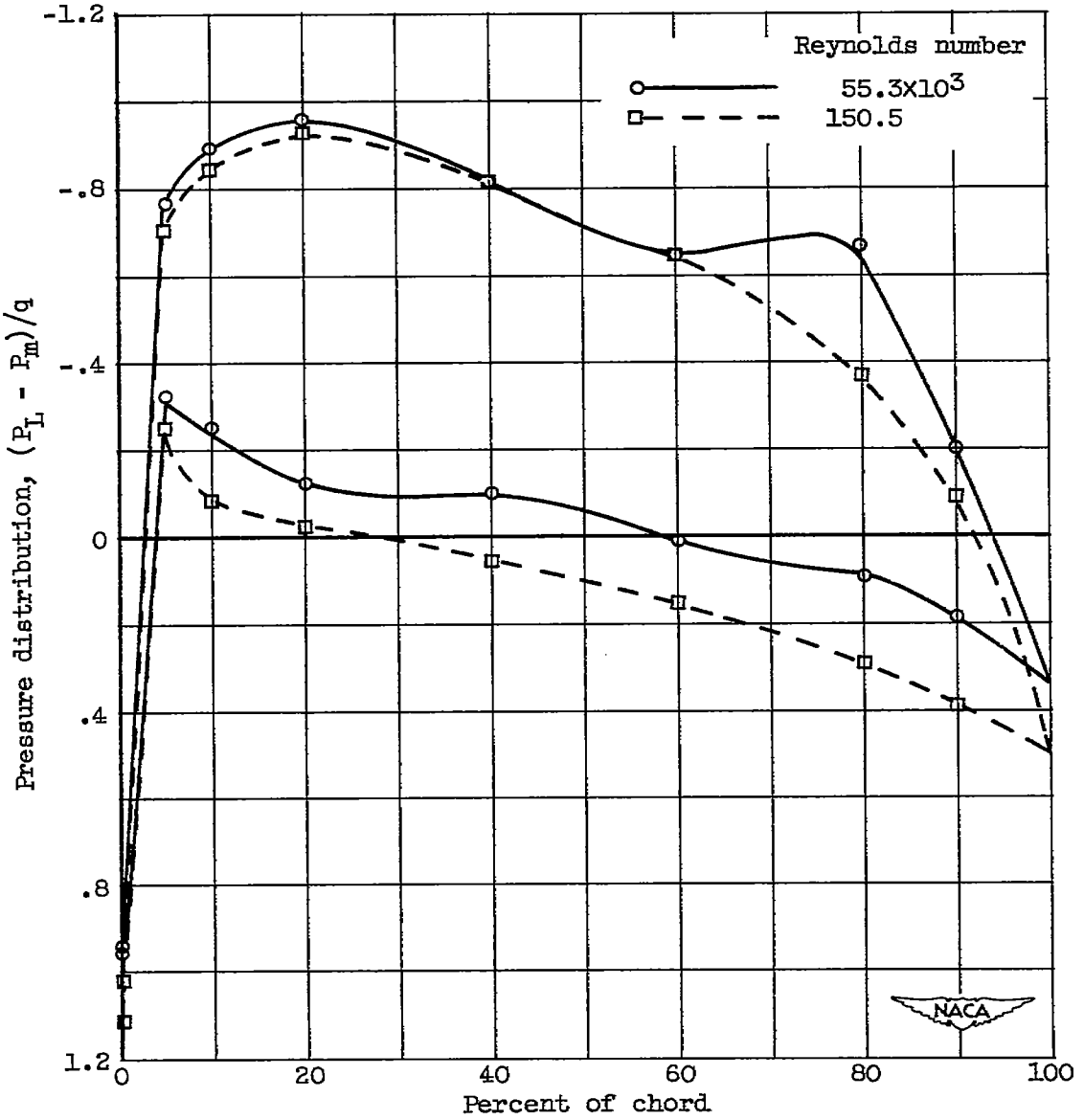

(b) Mean radius; angle of attack at mean radius, 15°.

Figure 8. - Continued. Pressure distribution around 65-(12)10 compressor blades.

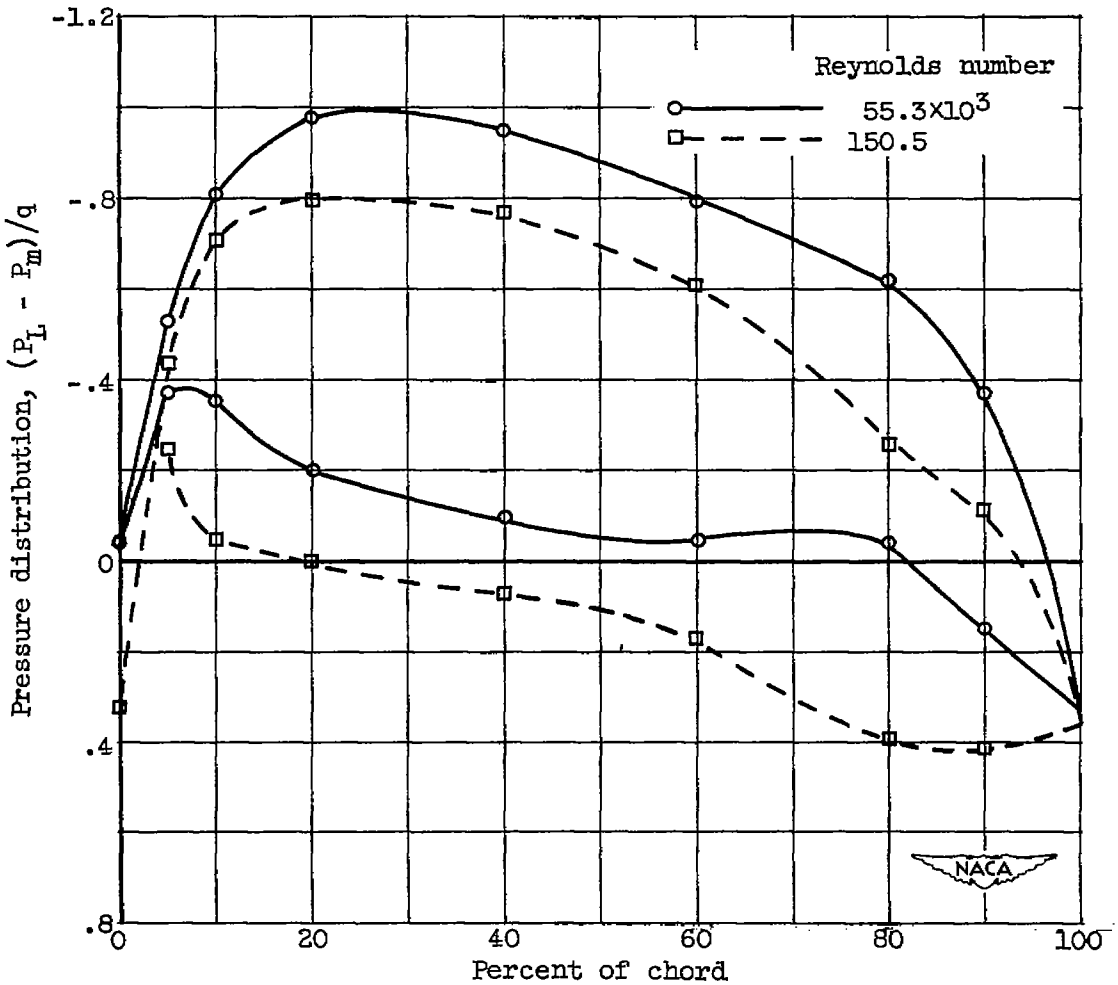

(c) Tip; angle of attack at mean radius, 15°.

Figure 8. - Continued. Pressure distribution around 65-(12)10 compressor blades.

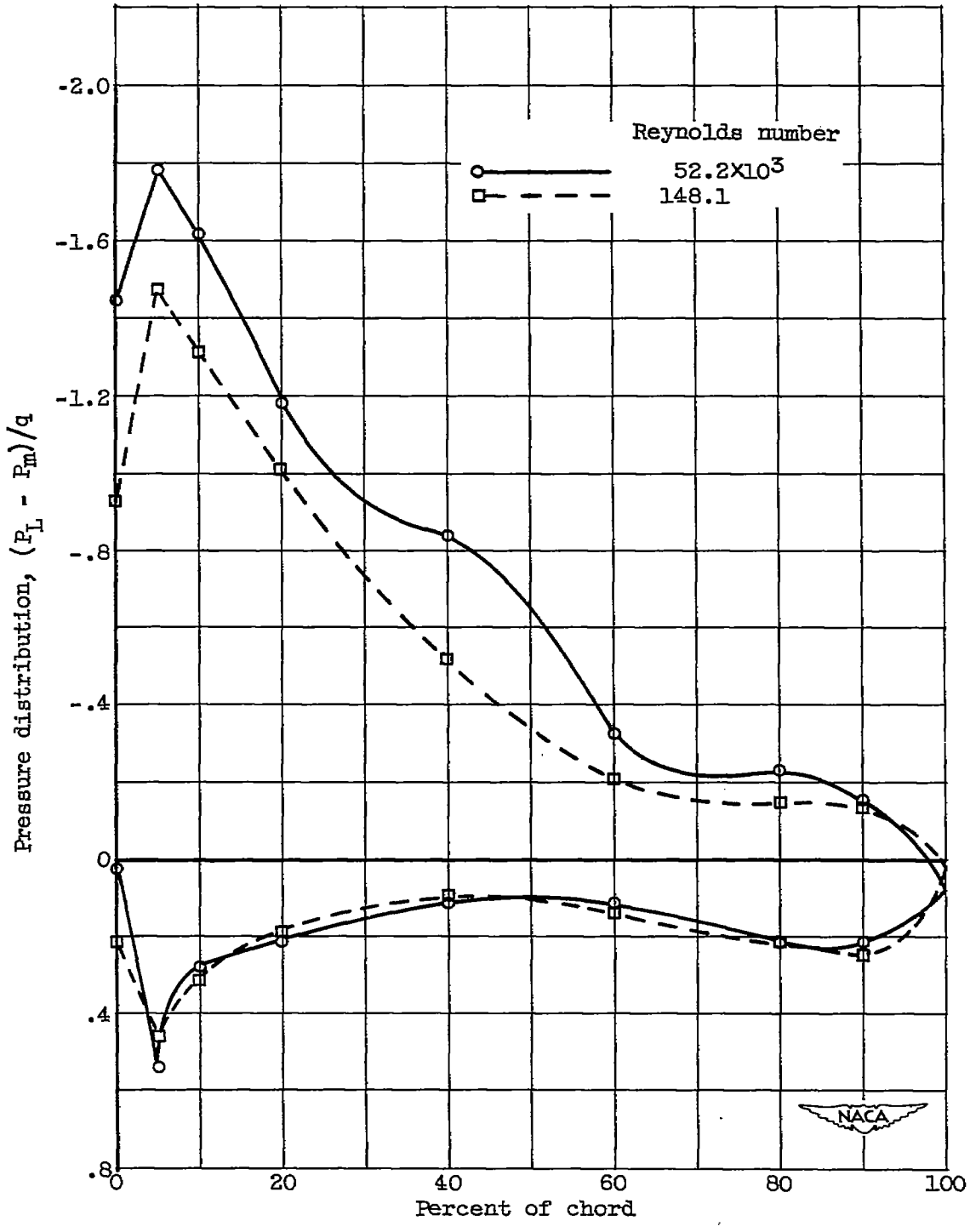

(d) Hub; angle of attack at mean radius, 25°.

Figure 8. - Continued. Pressure distribution around 65-(12)10 compressor blades.

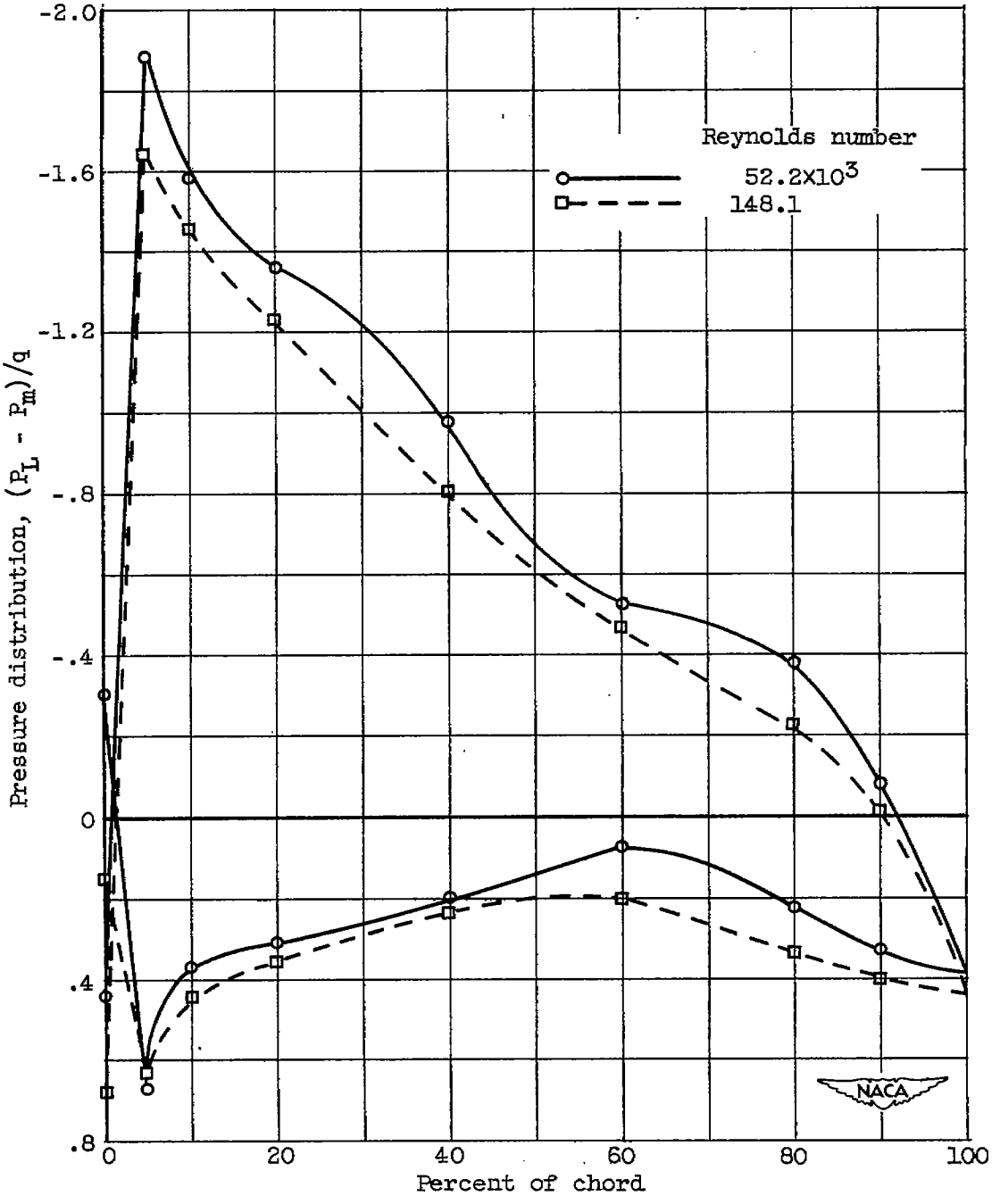

(e) Mean radius; angle of attack at mean radius, 25°.

Figure 8. - Continued. Pressure distribution around 65-(12)10 compressor blades.

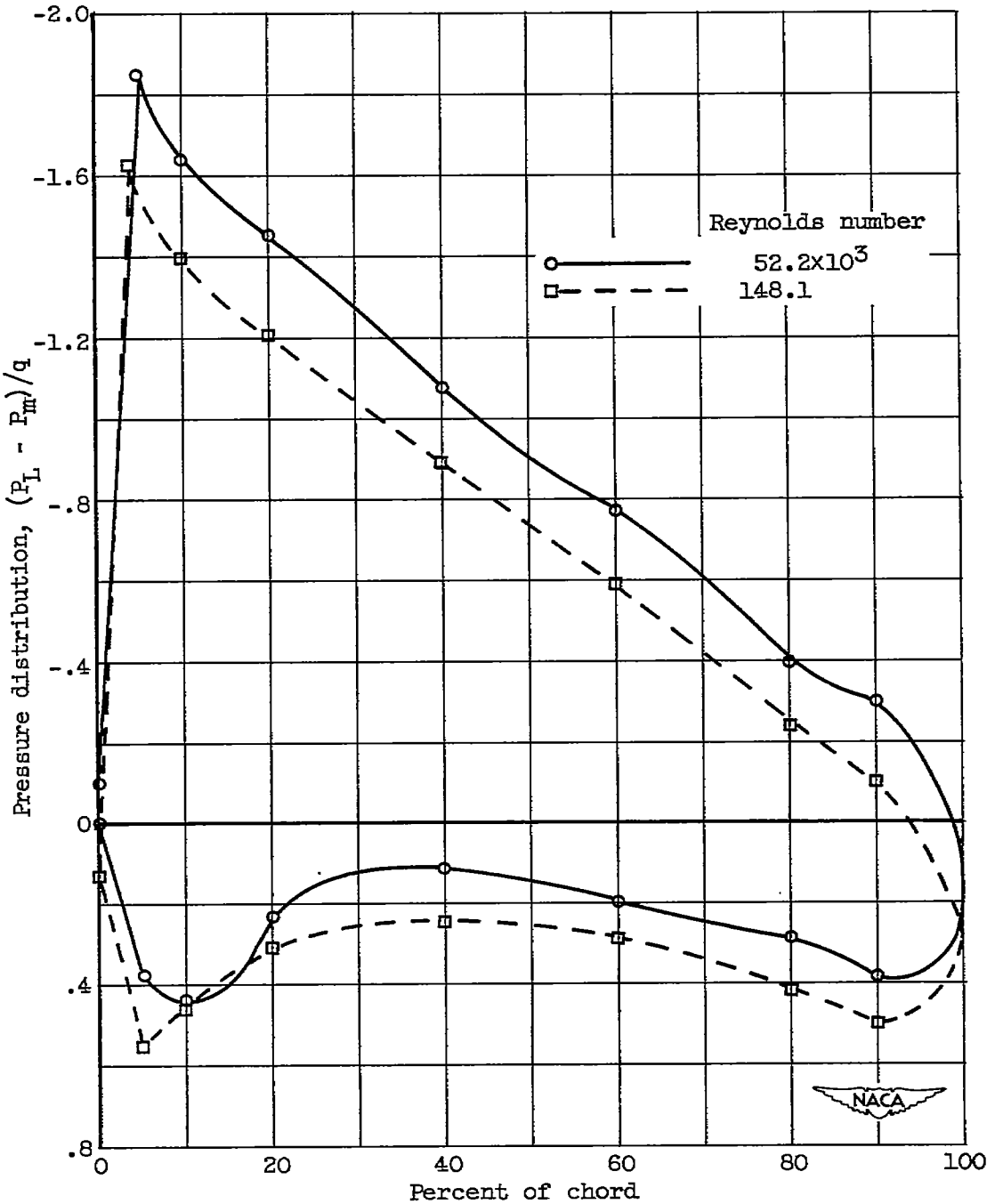

(f) Tip; angle of attack at mean radius, 25°.

Figure 8. - Concluded. Pressure distribution around 65-(12)10 compressure blades.

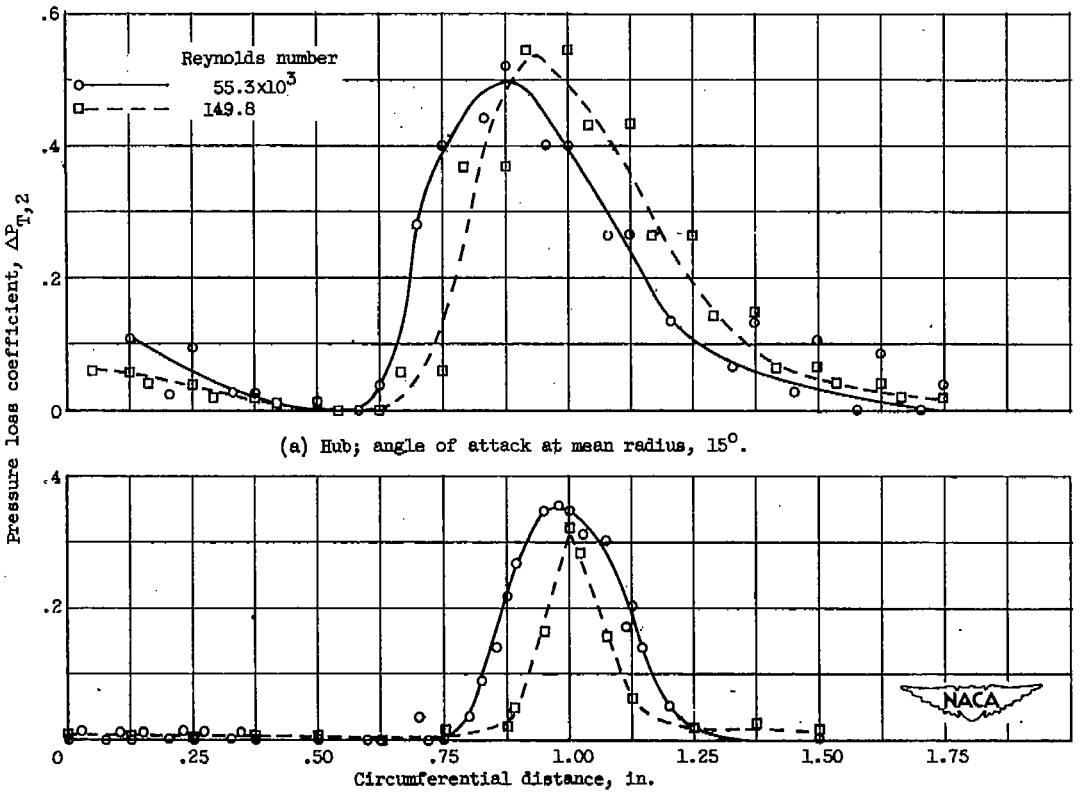

(a) Hub; angle of attack at mean radius, 15°.

(b) Mean radius; angle of attack at mean radius, 15°.

Figure 9. - Wake profile downstream of 65-(12)10 compressor blade.

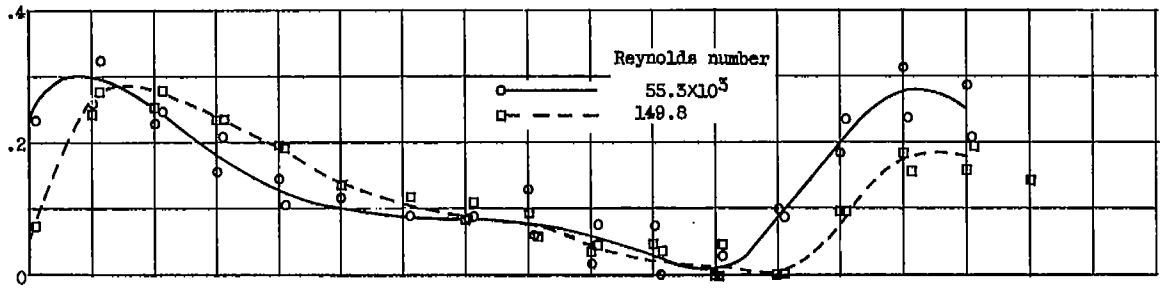

(c) Tip; angle of attack at mean radius, 15°.

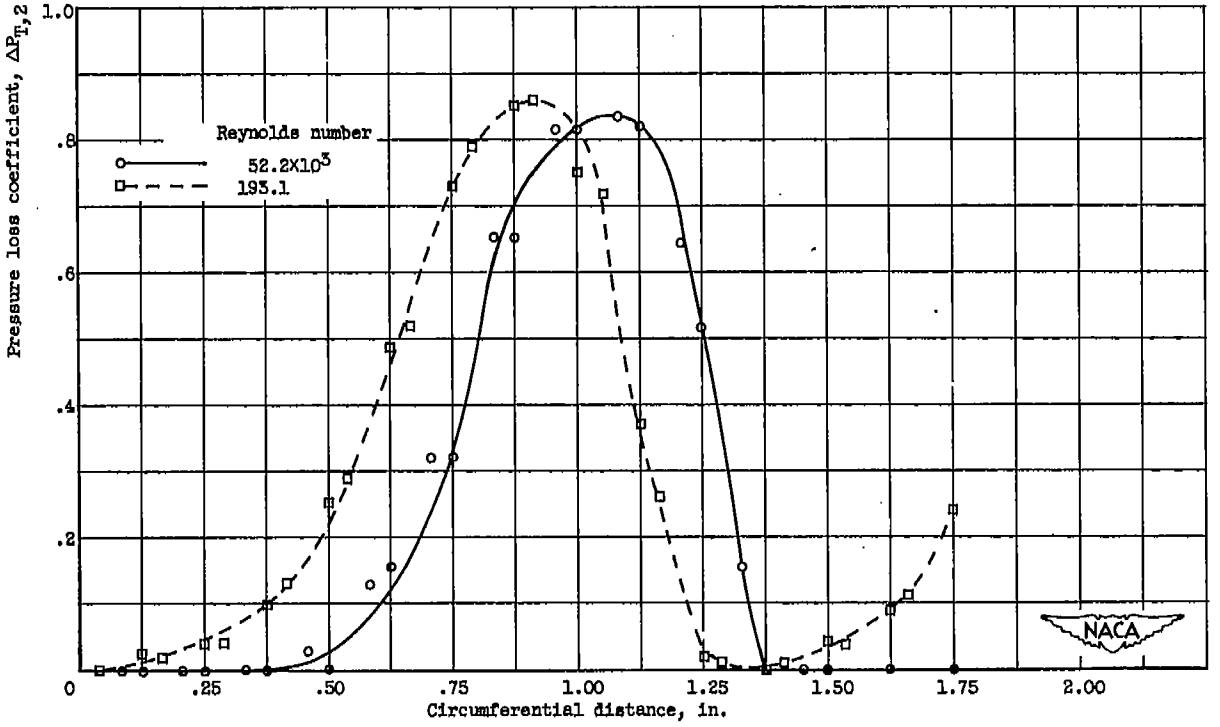

(d) Hub; angle of attack at mean radius, 25°.

Figure 9. - Continued. Wake profile downstream of 65-(12)10 compressor blade.

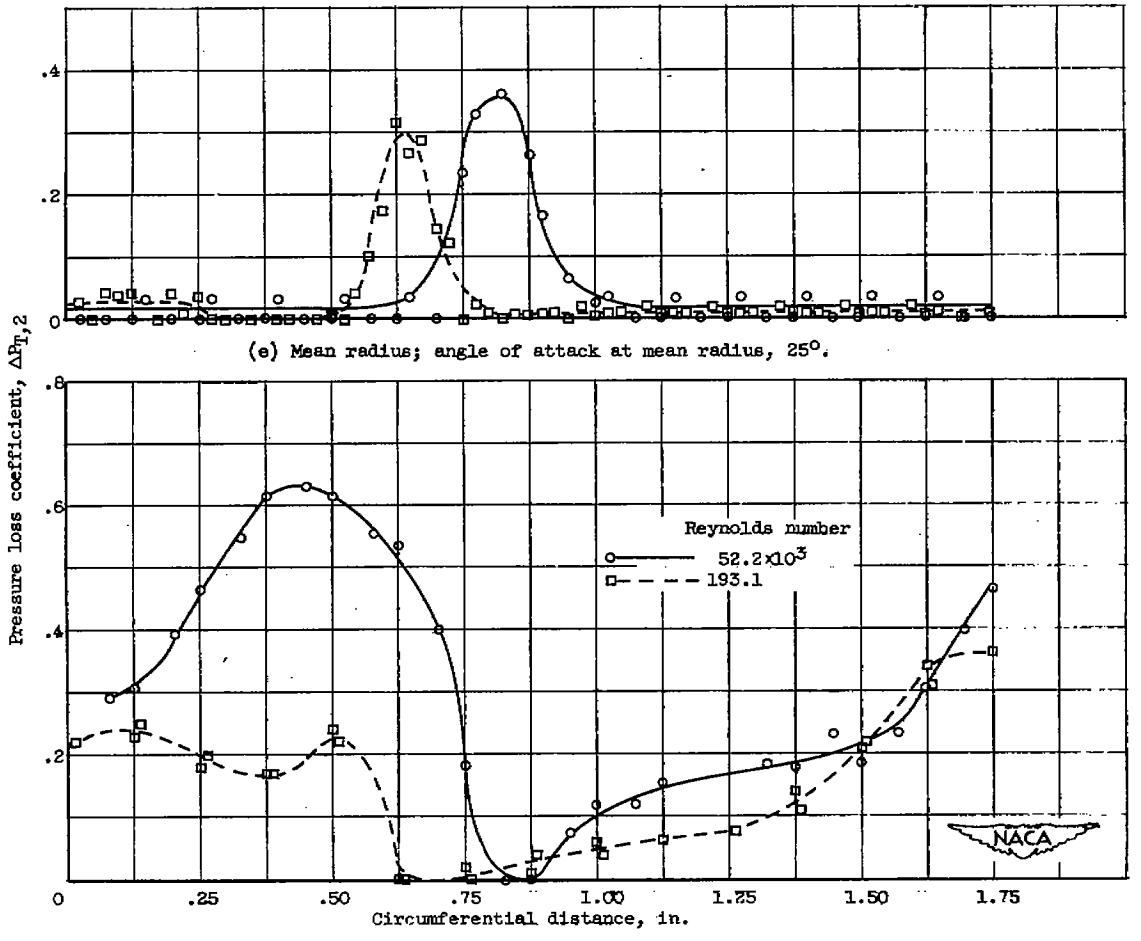

(f) Tip; angle of attack at mean radius, 25°.

Figure 9. - Concluded. Wake profile downstream of 65-(12)10 compressor blade.

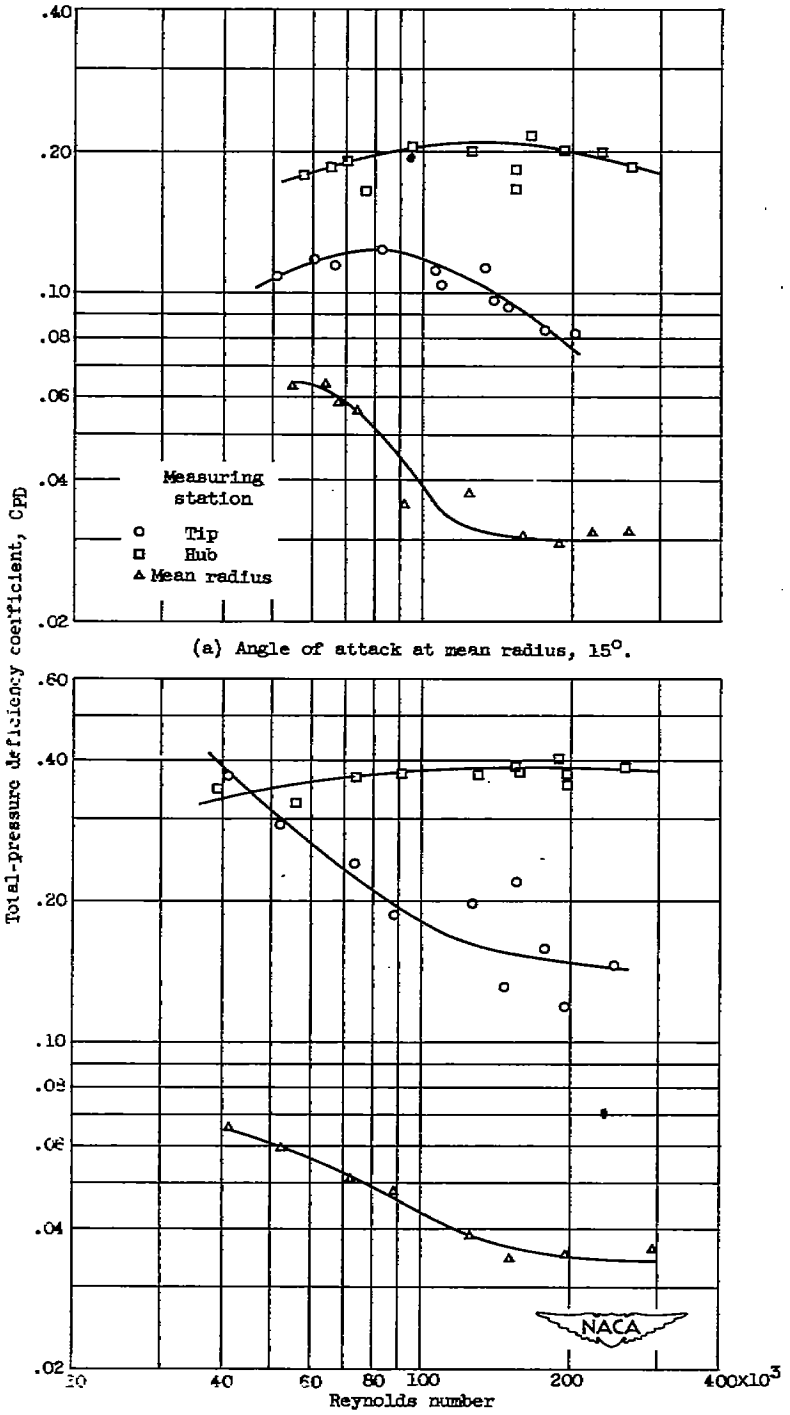

(a) Angle of attack at mean radius, 15°.

(b) Angle of attack at mean radius, 25°.

Figure 10. - Variation of total-pressure deficiency coefficient with Reynolds number.

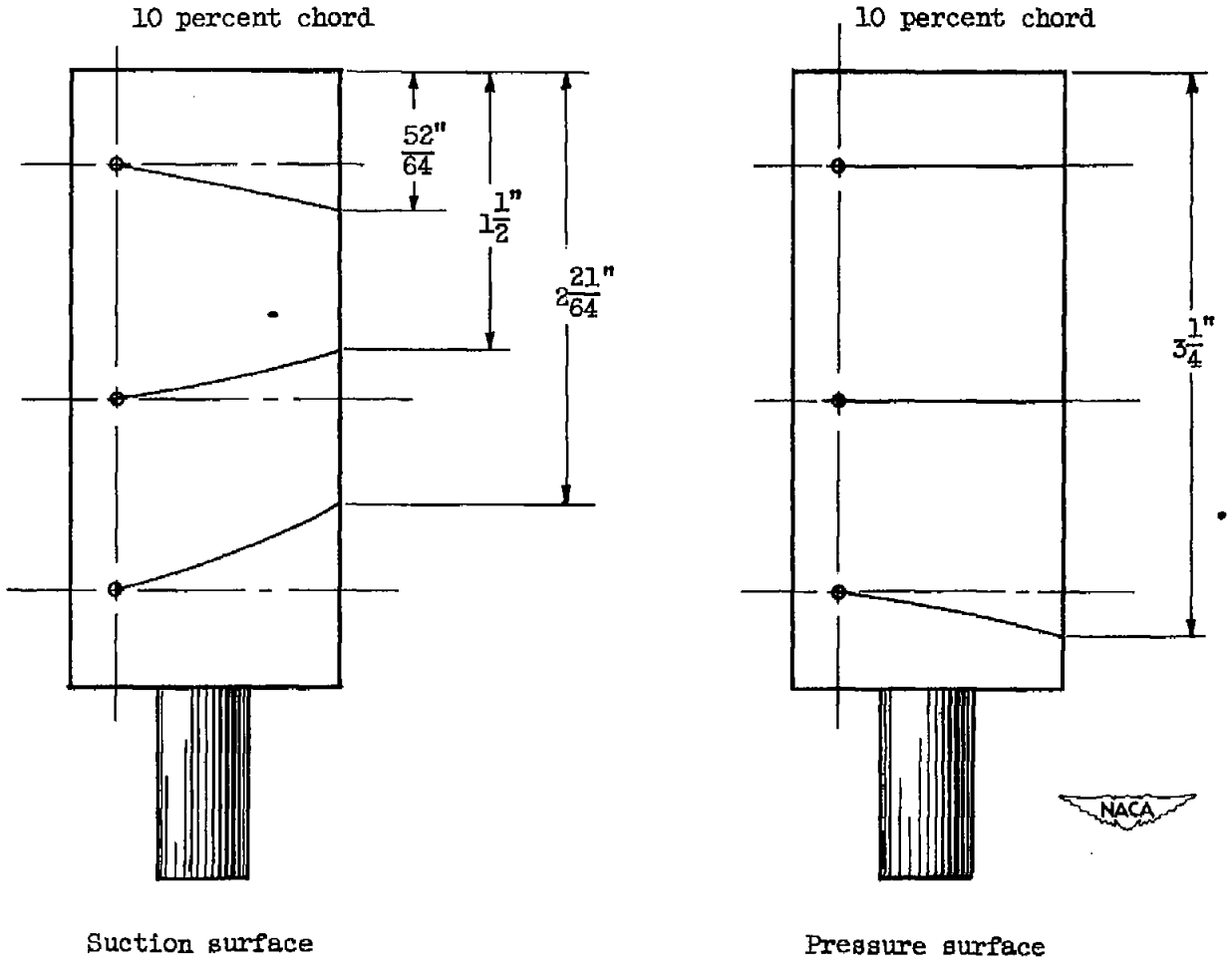

Suction surface

Pressure surface

(a) Reynolds number, 125,000.

Figure 11. - Diagram of chemically obtained traces on blade surfaces.

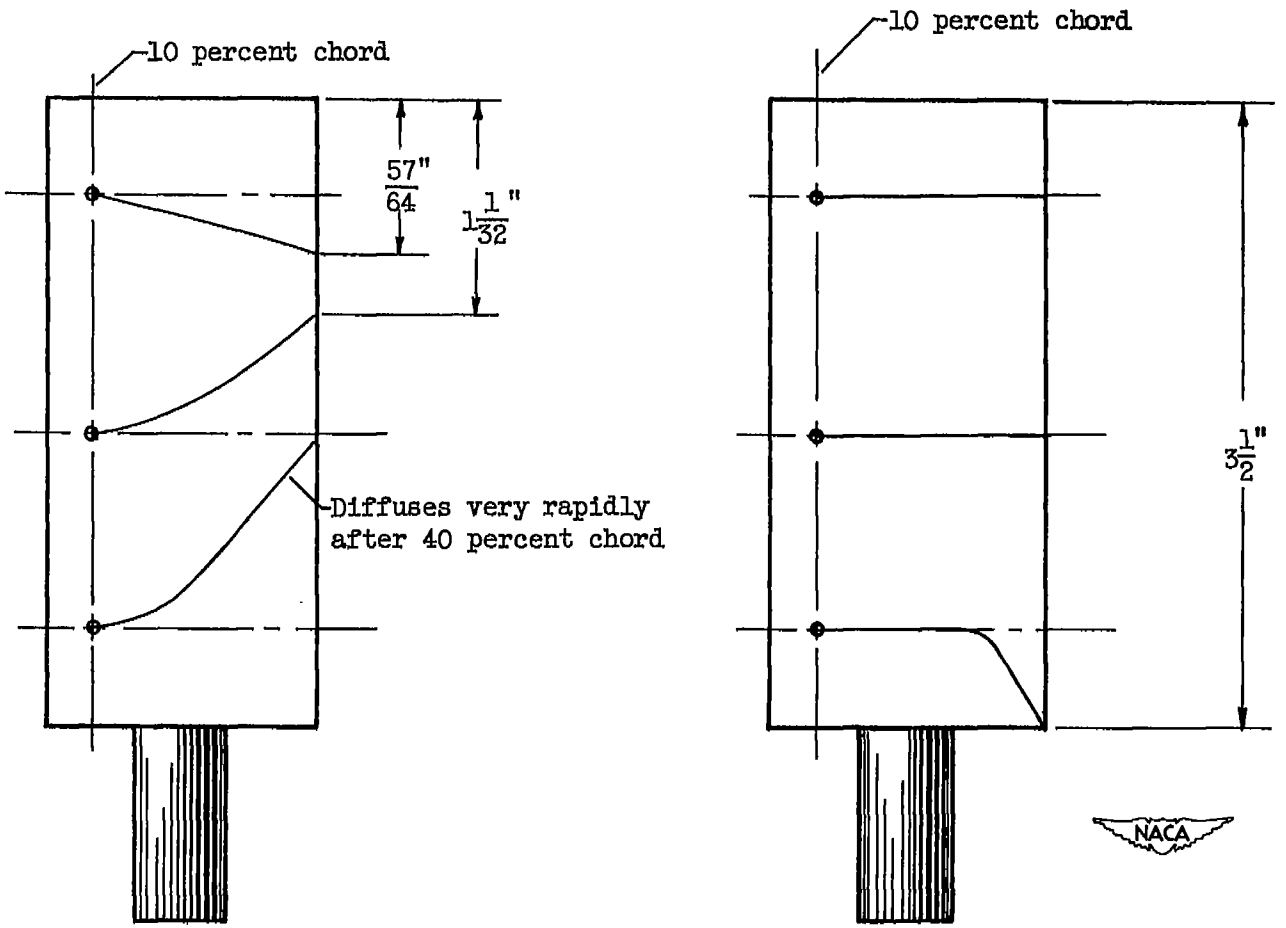

Suction surface

Pressure surface

(b) Reynolds number, 50,000.

Figure 11. - Concluded. Diagram of chemically obtained traces on blade surfaces.